



Material characterization and microstructural simulation of hollow spheres and PCM steel foams

B.H. Smith¹, S. Szyniszewski², J.F. Hajjar³, B.W. Schafer⁴, S.R. Arwade⁵

Abstract

The objective of this research is to characterize the mechanical properties of hollow spheres and PCM steel foams under compressive and tensile loading, and to develop and validate microstructural computational models for such foams that account for micro-scale buckling of the cell walls and localized material yielding. Such models allow the virtual investigation of the relationship between microstructural design parameters and macroscopic material properties. Steel foams are a new class of structural materials that have the potential to provide enhanced energy dissipation, stiffness, and buckling mitigation by virtue of their unusual mechanical properties. Through physical experiments we characterize some previously unreported properties of the material such as the compressive unloading modulus and its evolution with increasing plastic deformation, the Poisson's ratio of the material in the plastic range, and the tensile yield and fracture strengths. Our three dimensional finite element models are among the first to treat the material microstructure as random while incorporating both material and geometric nonlinearity at the micro-scale. The experimental characterization of the material properties feeds directly into work being performed to develop candidate applications of steel foam in civil structures, and the computational work is being used to suggest novel microstructural designs that lead to improved macroscopic material properties.

1. Introduction

Porous metals made from aluminum or titanium are becoming increasingly popular as stiff but lightweight materials for use in structural components of automobiles and aircraft. However, civil engineering applications require stronger and more economical materials than an aluminum or titanium foam can provide. Over the past decade, materials scientists have developed several ways to manufacture porous steel and a couple of these methods are now mature. However, the material's mechanical properties are not yet sufficiently defined to fully assess the potential structural applications of steel foams.

¹ Graduate Research Assistant, University of Massachusetts, Amherst, <bhsmith@engin.umass.edu>

² Post-Doctoral Scholar, Johns Hopkins University, <s.szyniszewski@gmail.com>

³ Professor and Chair, Northeastern University, <jf.hajjar@neu.edu>

⁴ Professor and Chair, Johns Hopkins University, <schafer@jhu.edu>

⁵ Associate Professor, University of Massachusetts, Amherst, <arwade@ecs.umass.edu>

Steel foam has strong potential in the structural engineering realm, particularly in enhancing stability, buckling resistance, and energy absorption capabilities. Traditional structural steel has proven itself invaluable as an engineering material, but the properties of structural steel have remained largely invariant for the past century. Steel foam offers designers the possibility of selecting their own desired elastic modulus and yield stress from a wide range of possible values, making use of excellent energy absorption properties, and employing highly advantageous strength to weight ratios. These advantages may be visually observed in the Ashby plots shown in Figure 1. Further, steel foam offers several non-mechanical properties which may prove advantageous to structural applications, including thermal resistance, sound and vibration absorption, and gas permeability.

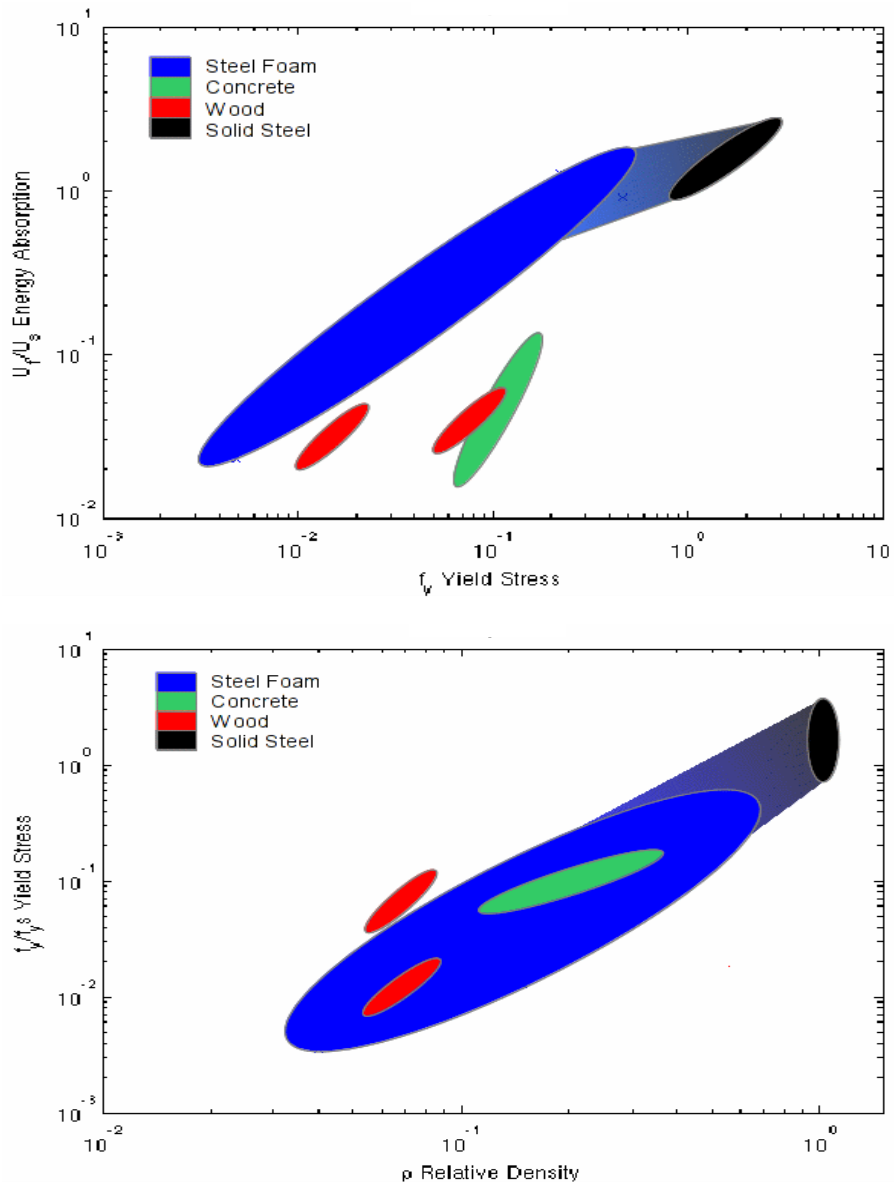


Figure 1: Ashby plots showing steel foam’s mechanical properties compared to solid steel, wood, and concrete. Note that the solid blue region represents data from published experimental tests, which is believed to extend continuously to that of solid steel, though high-density steel foams have not yet been tested. *Top*: Energy absorption vs yield stress. *Bottom*: Yield stress vs relative density.

Steel foams may be produced as either an isotropic or orthotropic material. Powder metallurgy and hollow spheres have proven to be the most promising isotropic production methods, while gasar and PCM methods represent the orthotropic methods. In this paper, hollow spheres and PCM methods are studied, including both experimental analysis and microstructural computer simulations. Previous research on steel foams has focused upon the compressive yield stress and densification strains (Fallet et al 2008, Gao et al 2007, Kari et al 2007). However, many more mechanical properties must be understood in order for the material to be effectively utilized in industrial applications. The additional material properties, which include compressive plastic Poisson's ratio, compressive unloading modulus, tensile elastic modulus, tensile unloading modulus, tensile yield stress, and tensile fracture strain provide sufficient information to allow calibration of a macroscopic, continuum, constitutive model for the material. This constitutive model is used in the evaluation of the collapse capacity of a steel foam core sandwich panel loaded in-plane. This example serves as a proof of concept for the use of continuum constitutive models for steel foam that are calibrated to experiments in compression and tension. The goal of developing computational micromechanics models, and validating them to experiments, is to be able to explore the microstructural design space of steel foams in a preliminary way while avoiding the high expense of material manufacture and testing.

2. Background Information

Hollow spheres metal foams feature one of the most consistent geometries possible in steel, they are isotropic, and they have the unique characteristic of having some voids completely closed (within the spheres) and some open to the atmosphere (interstitial between the spheres). The manufacturing method involves inserting polystyrene spheres into a liquid suspension of a binding agent and powdered steel, draining away the liquid, and then sintering the resulting material together under high temperature and pressure (Smith et al 2011).

PCM metal foams result in a controllable orthotropy, voids of consistent sizes, and very large range of possible densities from 5 to 100% that of solid steel. The process involves first manufacturing bimaterial rods having a shell of steel powder mixed with a binding agent, and a core having a forming filler such as a polymer mixed with a binding agent. These bimaterial rods are cut into set lengths, and then compacted either in a die or through an extruder. Finally, the resultant material is sintered in a furnace. During this final step, the filler material also melts out leaving the voids empty (Tuchinskiy 2005).

3. Experimental Testing

Two types of steel foam were tested experimentally: hollow spheres and PCM. Fifty bars of 14% relative density hollow spheres steel foam were acquired from the Fraunhofer Institute in Dresden, Germany. Each bar measures approximately 270mm by 52mm by 55mm and is composed of a mild steel of between 0.3% and 0.5% carbon. In addition, one block of 34% relative density PCM steel foam measuring 108mm by 108mm by 37mm composed of a high-strength steel was acquired from MER Corporation in Tucson, Arizona. The results of compression and tension tests are presented in this section.

The hollow spheres material could only be adequately machined using band saws, so all test specimens were prepared using this method. In contrast, the PCM block was easily milled, so test specimens were prepared by rough cutting on a band saw and then milling all surfaces.

3.1 Compression Tests

Three types of uniaxial compressive tests were performed in order to evaluate the mechanical properties of the available steel foam. Of these, all three were performed on the hollow spheres foam, while, due to the limited quantity of material available, only one was performed on the gasar foam. All tests were displacement-controlled and used an Instron 3369 testing machine with up to one extensometer. Tests were based upon standard ISO/DIS 13314 (“Compression Test for Porous and Cellular Metals”). The displacement rate was between 0.5mm/min and 1.0mm/min (0.3%/min and 1.3%/min) for hollow spheres tests and 1.5mm/min (10%/min) for PCM tests. Platens were lubricated with high-capacity automobile axle grease. At least three tests of each type were performed:

1. *Unloadings every 0.5% to 1.0% strain, longitudinal extensometer*
Hollow spheres dimensions: 52mm x 55mm x either 80mm or 140mm ($\pm 2\%$)
2. *No unloadings, transverse extensometer*
Hollow spheres dimensions: 52mm x 55mm x 75mm ($\pm 3\%$)
3. *No unloadings, reduced cross-section, no extensometer*
Hollow spheres dimensions: 25mm x 25mm x 55mm ($\pm 5\%$)
PCM dimensions with longitudinal pores: 9mm x 9mm x 14mm ($\pm 10\%$)
PCM dimensions with transverse pores: 11mm x 11mm x 17mm ($\pm 10\%$)

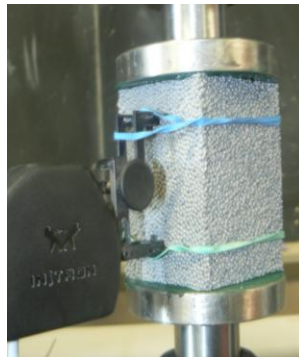


Figure 2: Photo of compression test on hollow spheres foam with longitudinal extensometer (test type 2).

3.1.1 Hollow Spheres Results

Comparing the longitudinal extensometer with the crosshead displacement data showed that there is a significant difference between the apparent stiffnesses calculated from each (3150 MPa versus 700 MPa), suggesting that this material experiences a particularly strong localized strain near the platens. Unloading moduli (test type 1) began around 2000 MPa in the elastic range, and rapidly increased to approximately 3150 MPa, a value from which there was minimal deviation with increasing strain (see Figure 3). Poisson’s ratio (test type 2) increased from zero or slightly negative to about 0.2 in the inelastic range, where the ratio appeared to level off between 20% and 50% strain (see Figure 4). Densification begins roughly at a strain of 65% and a stress of 17 MPa (test type 3, see Figure 4). Full results are summarized in Table 1.

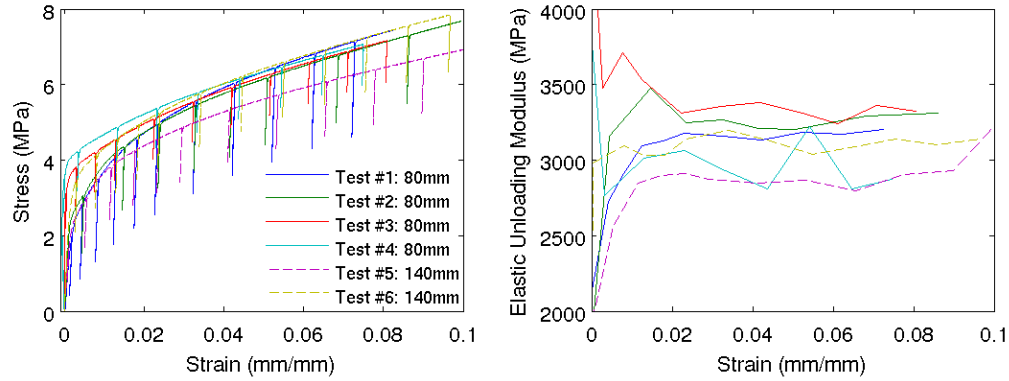


Figure 3: *Left*: Stress vs strain curves for unloading modulus test (test type 1). *Right*: Elastic unloading modulus vs strain, as measured manually from each unloading (test type 1).

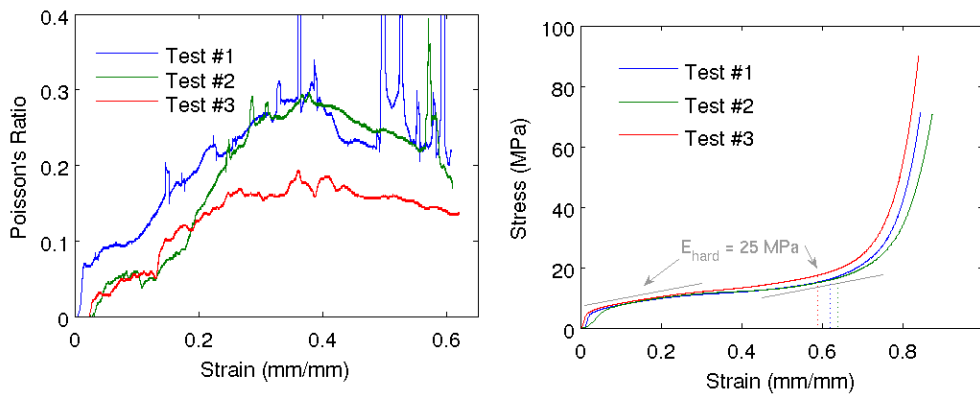


Figure 4: *Left*: Incremental Poisson's ratio vs Strain based upon 0.005 longitudinal strain increments (test type 2). *Right*: Stress vs strain curves for tests to densification (test type 3).

Table 1: Mechanical properties of hollow spheres steel foam in compression.

	Initial Loading Modulus (MPa)	Inelastic Unloading Modulus (MPa)	Yield Stress (MPa)	Densification Strain (mm/mm)	Densification Stress (MPa)	Elastic Poisson's Ratio	Poisson's Ratio 50% Strain
Average	1900	3150	3.6	65%	17	-0.05	0.2
Range	± 600	± 100	± 0.4	$\pm 5\%$	± 3	± 0.05	± 0.01

3.1.2 PCM Results

Due to material size being limited to a height of 37 mm and the smallest available extensometer being 51 mm, only tests without the extensometer were performed (test type 3). Note that this means that strain values shown in the summary graphs of Figure 5 are maximum strains, overestimating the actual strains by up to 50%. Due to the material's orthotropy, tests were performed both with the pores oriented longitudinally and with the pores oriented transversely between the platens. Results showed average yield stresses of 409 ± 10 MPa and 349 ± 50 MPa for longitudinal and transverse results, respectively. At an ultimate stress of roughly 500 MPa in both orientations, a diagonal shear crack instantaneously formed through the full width of the material. See Figure 5 for results graphs.

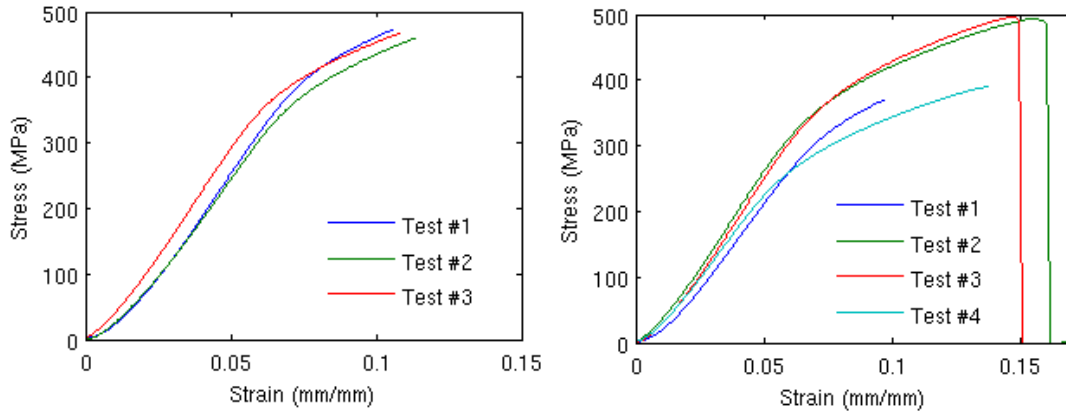


Figure 5: Stress vs Strain curves for tests to at or near ultimate compressive strength with pores oriented longitudinally (*left*) and transversely (*right*) to the platens. Strains shown are maximum strains and likely overestimate actual strains by up to 50%.

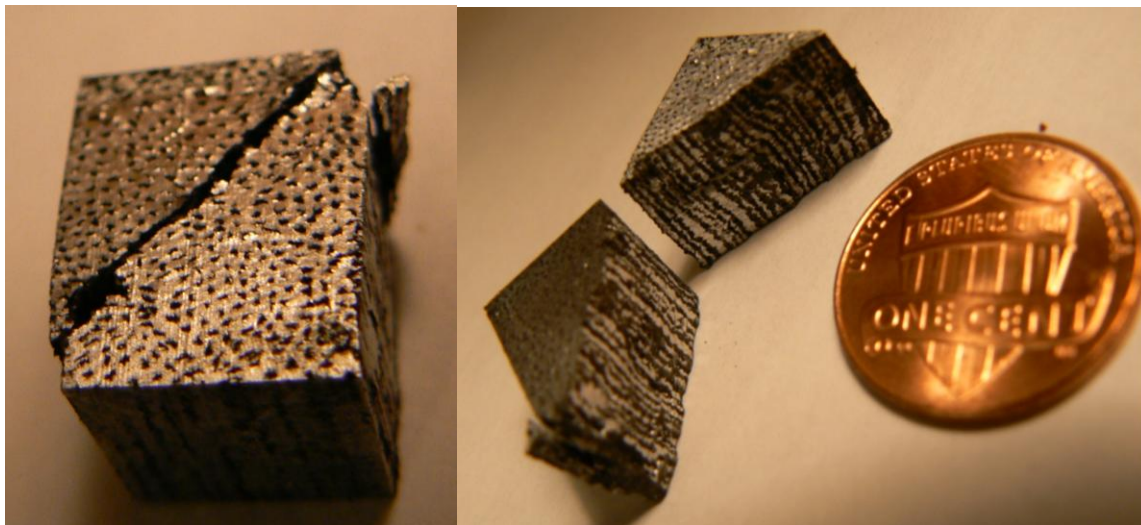


Figure 6: Photos of a transversely-oriented compression specimen after failure, showing the diagonal shear crack.

3.2 Tension Tests

In the absence of tensile test standards specifically designed for metal foams, tensile testing was based upon the ASTM E8-08 (“Tension Testing of Metallic Materials”) standard, and specifically the “plate-like” specimen described therein. For the hollow spheres tests, modified grips were designed, consisting of 25mm slots cut into both ends of the sample with solid plates epoxied into these two slots. Tension was applied at 0.5 mm/min (1.0%/min), and an extensometer was attached to the test section of the specimen (see Figure 7). Three hollow spheres samples were tested in this manner, plus a fourth was tested with repeated unloadings. For PCM tests, the “plate-like” specimen design could be used directly, but limited quantities of available material required the dimensions to be scaled down significantly. The specimens were cut to 6 mm thickness, with the testing section having a width of 15 mm and length of 11 mm ($\pm 3\%$). Wedge grips were used to directly hold the specimens (see Figure 7).

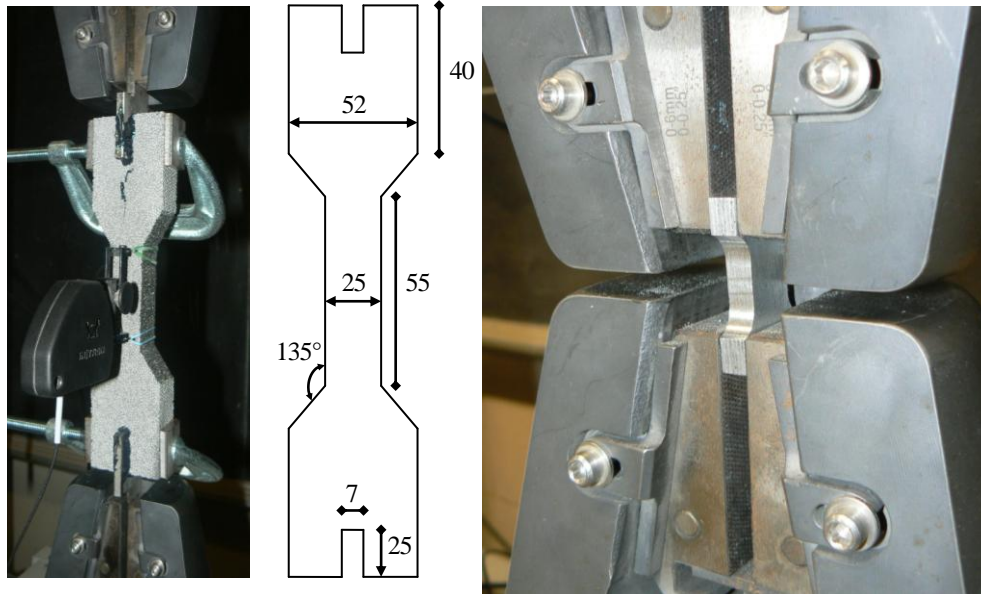


Figure 7: *Left:* Photo of a mounted hollow spheres tension specimen and dimensioned drawing (in mm, $\pm 3\%$).
Right: Photo of a PCM specimen mounted for testing.

3.2.1 Hollow Spheres Results

Tension tests for hollow spheres specimens showed a wide variation in results (see Figure 8). Fracture occurred at strains between 1.5% and 4.0%, and ultimate stresses were between 4 and 6 MPa. In tests #1 and #2, the fracture occurred along two distinct cracks (see Figure 8), while in test #3, the entire cross-section fractured across along a single dominant crack.

On a microstructural level, fracture surfaces were characterized by pullout of the sphere-to-sphere welds (see Figure 8). Unloading moduli were nearly identical to those observed in compression, at approximately 3100 MPa, but there was no evidence of lower moduli in the elastic range. Yield stresses were also within 0.1 MPa of compression results. Test results are summarized in Table 2.

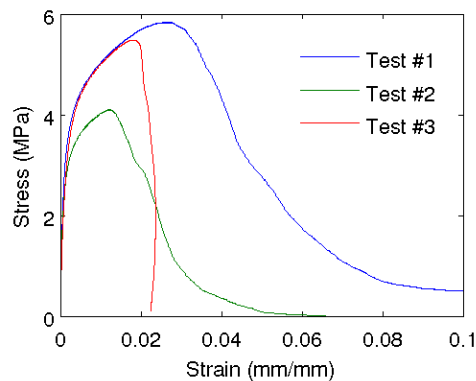


Figure 8: Stress-strain graph of regular tension tests performed, showing crosshead and extensometer measurements.

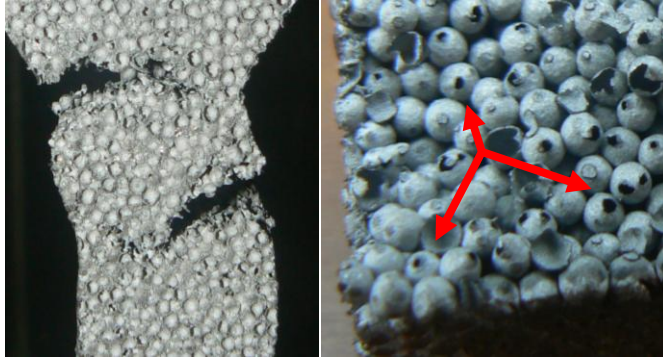


Figure 9: Left: Photo of fracture in test #1. Right: Macro photo of tensile fracture surface. Arrows mark examples of where welds pulled out.

Table 2: Summary of mechanical properties of hollow spheres foam in tension.

	Unloading Modulus (MPa)	Yield Stress (MPa)	Fracture Strain (mm/mm)	Fracture Stress (MPa)
Average	3100	3.5	2.3%	5.4
Range	±200	±0.4	±1%	±1.3

3.2.2 PCM Results

Tension tests for PCM materials were significantly more self-consistent than those observed in hollow spheres tests, but the tensile strength of the PCM foam was observed to be nearly three times lower than its compressive strength. Two tests each were performed with the pores oriented longitudinally and transversely to the wedge grips. The transverse orientation was roughly 50% weaker than the longitudinal direction. As in compression, the PCM specimens were too small to attach an extensometer to, so strain values shown in the results graph of Figure 10 are maximum values, and may exceed the actual strain values by up to 600%.

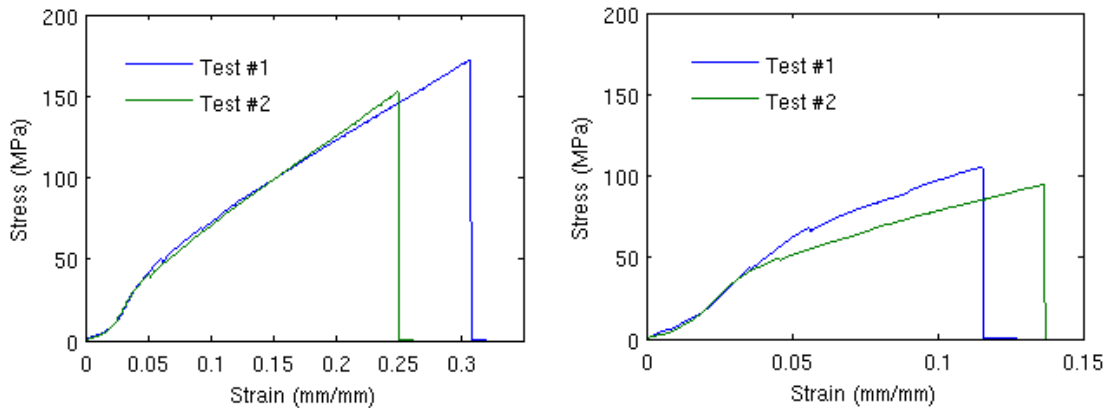


Figure 10: Tension test results for PCM steel foams with pores oriented longitudinally (*left*) and transversely (*right*) to the wedge grips. Strains shown are maximum strains and may be inaccurate by up to 600%.

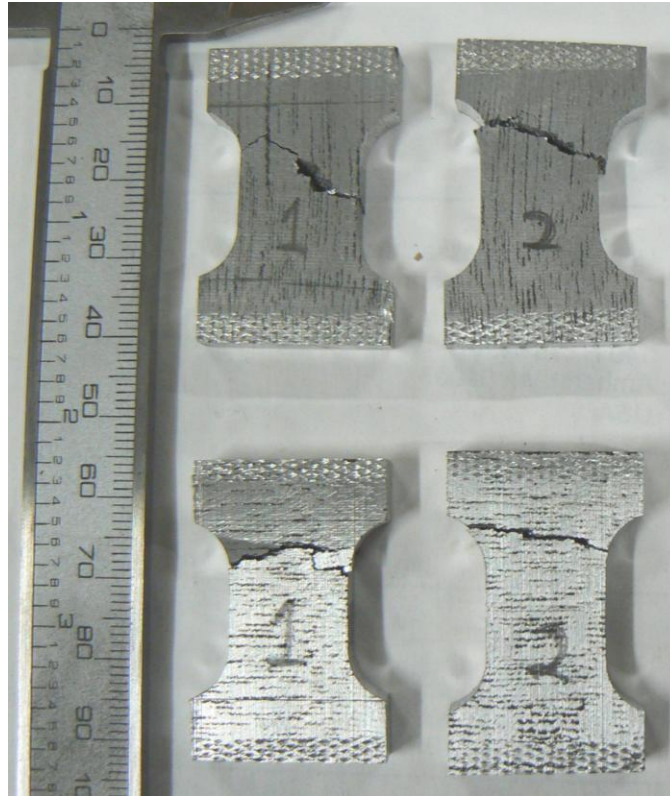


Figure 11: Photo of tested longitudinal (top) and transverse (bottom) PCM tension specimens.

3.3 Hollow Spheres Discussion

Gibson and Ashby (Ashby et al 2000) developed mathematical models for predicting the effective properties of metal foams. Comparing all of their available “open-cell” equations to experimental results, the results are within the very large predicted possible range with the exception of Poisson’s ratio, which is predicted to be approximately 0.3, differing substantially from these results.

Tension and compression feature different yielding and failure modes, with the compressive strength depending upon wall buckling, and the tensile strength depending upon weld size and quality as well as sphere shell tension. It is believed to be a coincidence that the tensile and compressive yield strengths are actually almost the same (averaging 3.4 or 3.5 MPa).

Due to compression required during the manufacturing process in order to sinter the material, the spheres themselves have significant deformities, as can be seen in the microstructural images of Figure 12. These deformities encourage buckling of the spheres and are a microstructural instability.

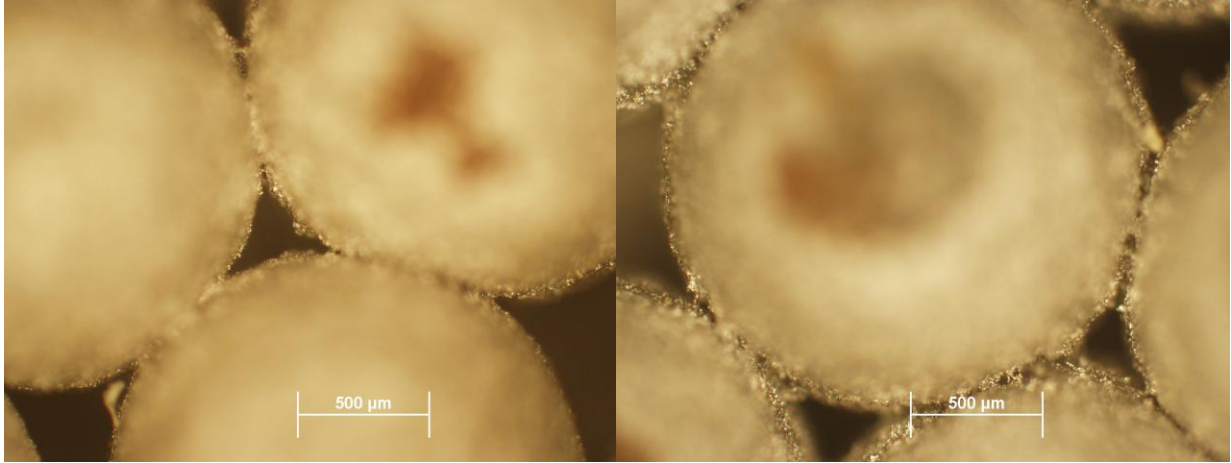


Figure 12: Two microstructural photos of hollow spheres showing the amount by which spheres are deformed around weld regions, resulting in instability in the spheres walls.

3.4 PCM Discussion

The PCM material has proven to be significantly more brittle than the hollow spheres foam. While precise ultimate strains were not determinable, they were less than 15% in both tension and compression. The brittleness arises from the sintering process during manufacturing.

The ability to mill the PCM material led to smooth surfaces and few macroscopic crack initiators, but cracks began at the pores instead, as was particularly visually apparent in tests where pores were oriented transversely.

4. Computational Models

Computational models have been developed using MatLab and ADINA to simulate the behavior of hollow sphere and PCM foams. A different geometry generation algorithm is used for each manufacturing method. All models are meshed with either 10-node or 11-node tetrahedral elements, and available computing power limits the maximum size to approximately 6 or 7 mm cubes. These cubes consist of about 360,000 elements resulting in over 3 million degrees of freedom. In hollow spheres simulations, the number of elements is tightly tied to the thickness of the spheres, which is approximately 0.08 mm in these simulations. In PCM simulations, the element size is determined by the smallest dimension of the internal pores. Each simulation of a 6 mm cube of material takes approximately 12 hours to run on a 24-core, 2.4 GHz per core, 76 GB RAM machine.

Post-processing is performed using purpose-written MatLab code. Raw nodal displacements and reaction forces are imported into MatLab and then either summed or averaged to determine stresses and strains. Poisson's ratio is determined by dividing the average transverse strain over a given increment of longitudinal strain by that longitudinal strain increment.

4.1 Hollow Spheres Geometry Generation

The microstructure of sintered hollow spheres foam consists of the spheres and the welds between those spheres. The spheres have been shown to be random close-packed (RCP) (Gao et al 2008). Wouterse and Philipse (2006) tested five RCP algorithms, and showed that two different variations of the "Mechanical Contraction Method" resulted in RCP stackings that were

most similar to an experimental stacking. The simpler of those two algorithms, the “Modified Mechanical Contraction Method”, was selected (Wouterse and Philipse 2006, Kansal et al 2002).

Welds between spheres are modeled by means of allowing a set amount of overlap between spheres and then adding a squat cylinder on top of that overlap region to ensure that none of the original spheres’ mass is lost. Several variables are allowed to vary randomly in this geometry algorithm; these include the sphere size, wall thickness, and sphere location (see Table 3). In the absence of any studies to show otherwise, normal distributions truncated at zero are assumed for all random parameters. See Figure 13 for an example of the geometry generated by this algorithm.

Table 3: Main geometric input parameters for hollow spheres simulations.

Input Parameter	Probabilistic Distribution
Sphere radius	Gaussian
Sphere wall thickness	Gaussian
Weld overlap	Deterministic
Initial sphere placement	Deterministic (face-centered cubic), or Uniform random
Number of spheres	Deterministic

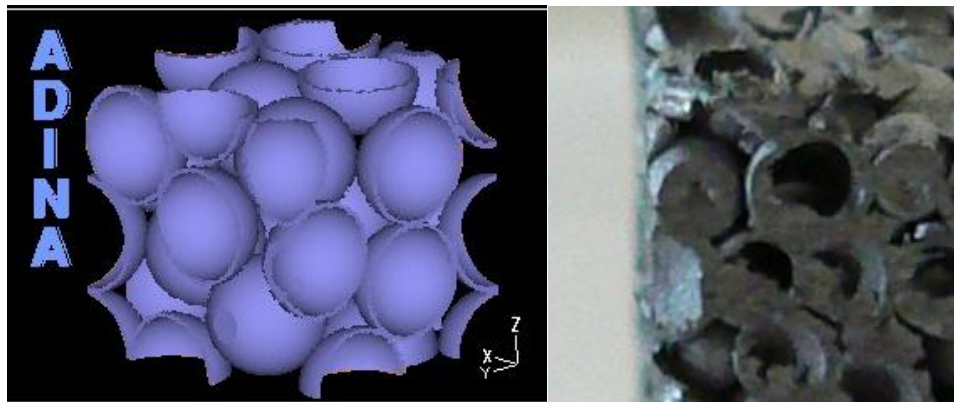


Figure 13: *Left*: Sample image of the geometry in a hollow spheres simulation. This specific geometry precisely represents the material upon which experiments were performed. *Right*: A macro photo of the material which was tested experimentally.

4.2 PCM Geometry Generation

The PCM geometry algorithm was targeted at accurately representing metal foams produced by the gasar, powder metallurgy, and high-density composite hollow spheres methods in addition to PCM. To represent all of these adequately, the model uses cylinders with hemispherical caps for the void geometry. These cylinders may then be oriented at any angle and elongated as necessary. The void centroids are modeled as a Poisson point field, or when overlap of the voids must be restricted, as a hard-core Poisson point field.

The length of the void and the diameter of the void cylinder are both modeled as Gaussian random variables. The orientation in spherical coordinates of the voids is modeled as two Beta random variables. The geometry then also allows the minimum distance between voids to be

adjusted as a deterministic variable. See Table 4 for a summary of these parameters. The resulting relative density depends upon the number of voids, void length, and diameter parameters. Upon completion, this algorithm results in a geometry such as that displayed in Figure 14.

Input Parameter	Probabilistic Distribution
Void length	Gaussian
Void diameter	Gaussian
Void orientation θ	Beta ($0 - \pi$)
Void orientation ϕ	Beta ($0 - 2\pi$)
Minimum void distance	Deterministic
Number of voids	Deterministic

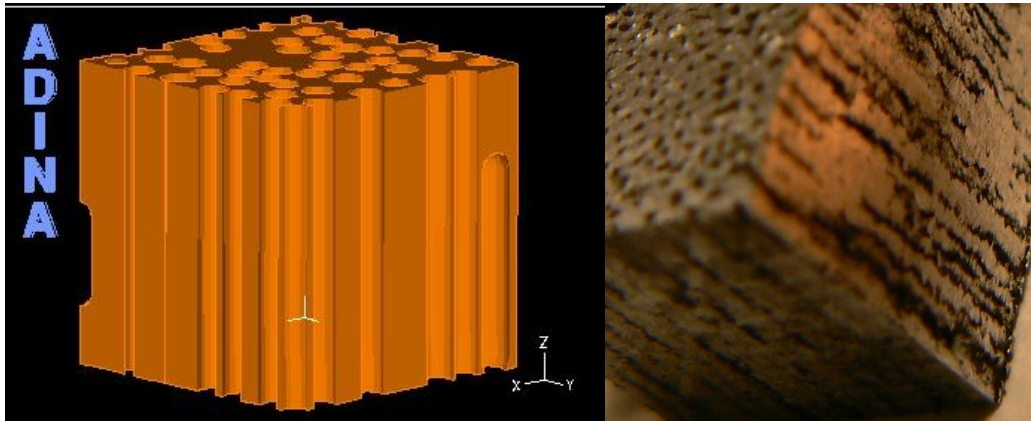


Figure 14: *Left*: Sample image of the geometry in a PCM simulation. *Right*: A macro photo of the material which was tested experimentally.

4.3 Hollow Spheres Validation

Several simulations have been performed to validate the accuracy of the models by comparison to experimental results. Model input parameters, such as sphere and weld size for hollow spheres geometries or void size and spacing for PCM geometries, were determined by either direct measurement or approximation and then random geometries were generated by the simulation code. With the code validated, parameter studies can then be performed, running a series of simulations to investigate the effects of changing various geometry parameters upon mechanical properties.

The hollow spheres geometry was validated against the experimental tests as described in section 2 of this paper. Compression test simulations were performed to 10% strain, and resulted in elastic moduli within 10% of experimental and yield stresses within 25% of experimental. Some inaccuracy is expected due to the small, 6mm, size of the simulated samples. Samples smaller than 6 void diameters have been shown to be inaccurate, and samples of the 3 void diameters used in the simulation are estimated by Andrews et al (2001) to be inaccurate by up to about 25%. Further, the microporosity within the sphere walls is not precisely known and the effects

thereof are only estimated. This last point probably had the greatest effect upon the inaccuracies in the first two simulations, as shown in Figure 15.

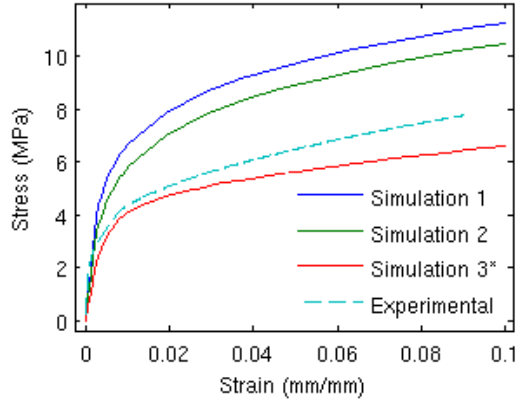


Figure 15: Validation simulations for hollow spheres uniaxial compression. Simulations #1 and #2 used the same parameters set, but with different random seeds. Simulation #3 additionally used a lower base yield stress but otherwise identical parameters.

4.4 Hollow Spheres Sensitivity Analysis

Using the hollow spheres validation simulation described in section 3.2.1 as the basis point, a sensitivity analysis was performed to explore the effects of varying specific microstructural parameters. The varied parameters are those which could be adjusted in the actual manufacturing process, including base metal yield strength, sphere diameter, sphere shell thickness, and sphere overlap distance. The last represents and is physically equivalent to the amount of pressure applied during the sintering process.

Three points were simulated for each parameter in order to acquire sensitivities: the central value, one slightly below, and one slightly above. Sensitivities were defined by first-order central differences normalized to the central value of elastic modulus of yield stress (see equations 1 and 2, respectively, where p is the varied parameter). At each point, one simulation was performed with a deterministic, face-centered cubic (FCC) geometry (see Figure 16), and two were performed with random geometries. All other parameters were set as deterministic. It is important to note that when varying the sphere diameter or the sphere shell thickness, this also changed the relative density of the material, so some of the change in mechanical properties is due to there simply being more or less mass within the volume. Further, the relative density of a specimen with a random geometry is lower than that with a face-centered cubic geometry.

$$E_{norm} = \frac{E_{upper} - E_{lower}}{(p_{upper} - p_{lower}) \cdot E_{central}} \quad (1)$$

$$f_{y,norm} = \frac{f_{y,upper} - f_{y,lower}}{(p_{upper} - p_{lower}) \cdot f_{y,central}} \quad (2)$$

In the results, it was observed that the variation was close to linear for most parameters over the range simulated, though became noticeably non-linear when varying the sphere diameter, as can be see from the graphs in Figure 17. The first-order central differences are shown in Table 5.

By utilizing these sensitivity results from computational simulations, the optimal material characteristics for a desired combination of elastic modulus and yield stress may be determined. With more such simulations, it would be possible to determine the material properties needed in order to achieve any mechanical properties within the range afforded by the hollow spheres method. Should an organization desire a material with a certain set of physically possible properties, they could simply consult the formula and determine the manufacturing parameters needed to achieve them.

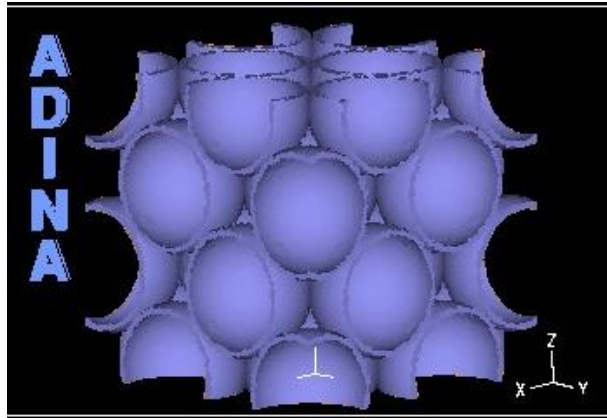


Figure 16: Sample image of a face-centered cubic (FCC) simulation geometry.

Table 5: First-order central difference results from the sensitivity analysis.

Varied Parameter	Central Value	Elastic Modulus (E_{norm})		Yield Stress ($f_{y,norm}$)	
		FCC	Random	FCC	Random
Base Yield Strength	262 MPa	0.000	0.000	0.004	0.002
Sphere Diameter	1.86 mm	-1.91	-1.08	-2.04	-0.75
Shell Thickness	0.083 mm	12.08	15.96	10.97	14.68
Weld Overlap	0.04 mm	10.31	0.56	10.97	2.77

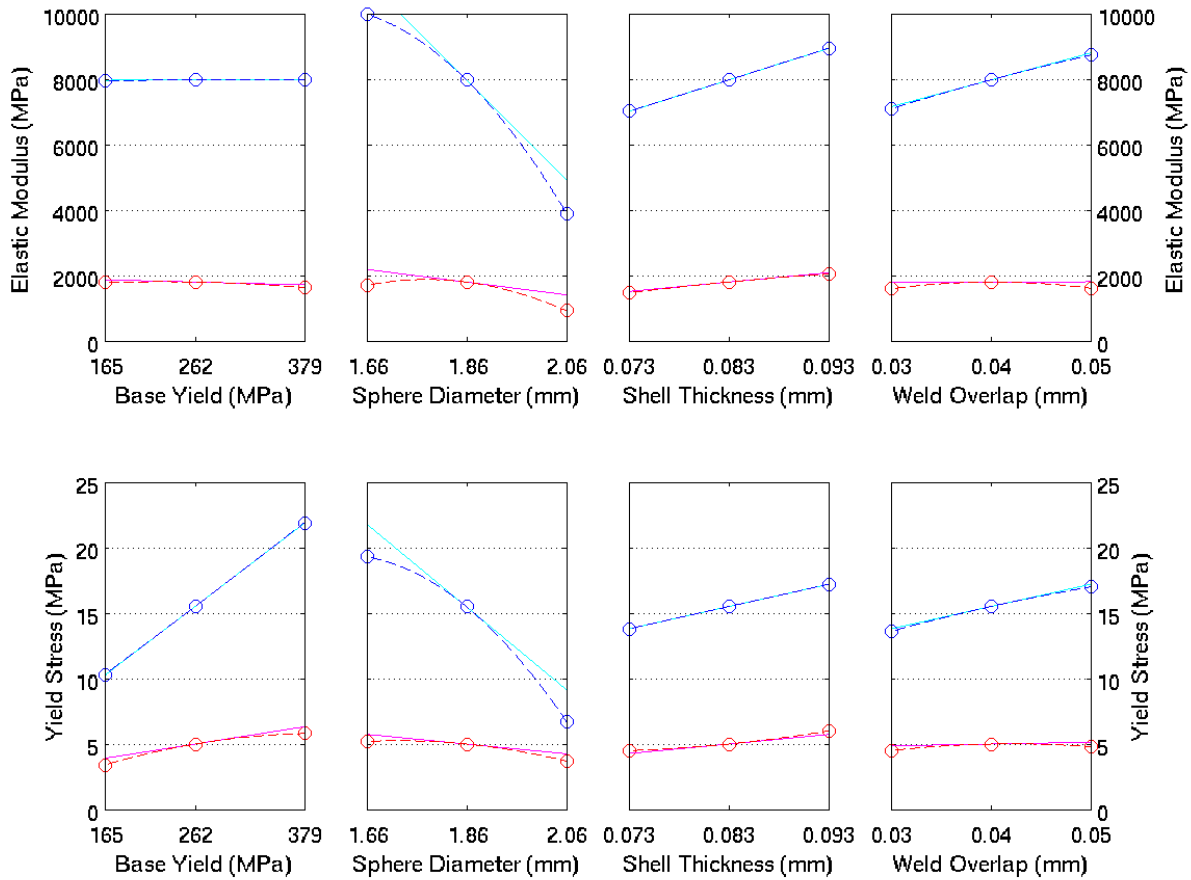


Figure 17: Graph of all simulations performed in sensitivity analysis. Blue points are FCC simulations; red points are the average of the two random simulations performed at each point. The first-order central difference slopes are shown as solid lines, and the second-order curve fits are shown as dashed lines.

5. Applications to Structural Components

5.1 Macroscopic Constitutive Modeling

Macro-scale finite element models utilizing solid or shell elements may employ homogenized properties such as elastic modulus, yield stress, etc. but this will only lead to an accurate material response representation up to initial yield. Classical von Mises plasticity utilizing associated flow rules typically assume incompressibility in the plastic regime and that yield properties are dependent only on shear stress (distortional energy) (Khan 1995). However, steel foam is compressible in the plastic regime and thus mean stress is important (dilatational energy).

Miller (2000) and Deshpande and Fleck (2000) generalized von Mises plasticity by accounting for pressure dependence in their effective stress formulation. The model was expanded and validated for aluminum foams by Reyes et al. to include nonlinear hardening, and later to also account for tensile fracture (Reyes 2003, Hanssen et al 2002). Our experiments provided data for calibration of Deshpande-Fleck plasticity and enabled simulations of structural components.

5.2 Structural Component Modeling

Experimentally calibrated plasticity models enabled capacity evaluation of sandwich plates with a steel foam core and steel face sheets. Numerical simulations accounted for material and geometric nonlinearity. Simply supported panels with in-plane compressive loading applied at opposite plate edges were loaded up to buckling collapse. Yield initialized at the center of the concave face sheet. It spread toward the unloaded edges. Immediately after the yield propagation reached the supported sides, plastic collapse of the panels was observed. Plasticity localized in a single half-wave (see Figure 18).

Numerical simulations enabled the search for an optimal balance of material between steel face sheets and a foamed core. The benefits of sandwich panels for plate buckling mitigation are remarkable, particularly for slender plates with width to thickness ratio greater than 100 (see Figure 19). Sandwich panels with optimized characteristics increased buckling collapse capacity by 2 to 4 times in comparison to slender steel sheets of the same weight.

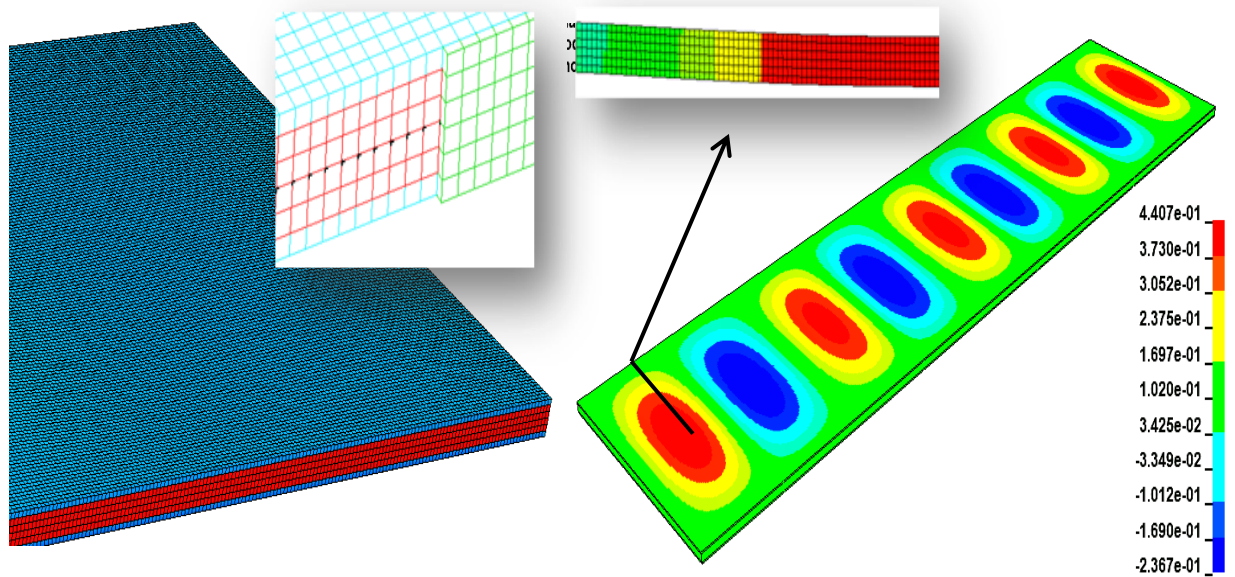


Figure 18: Finite element model of a simply supported steel foam sandwich panel plate under in-plane compression, with steel face sheet and steel foam core are modeled with brick elements in LS-DYNA. Mesh is shown on the left and typical results are shown on the right.

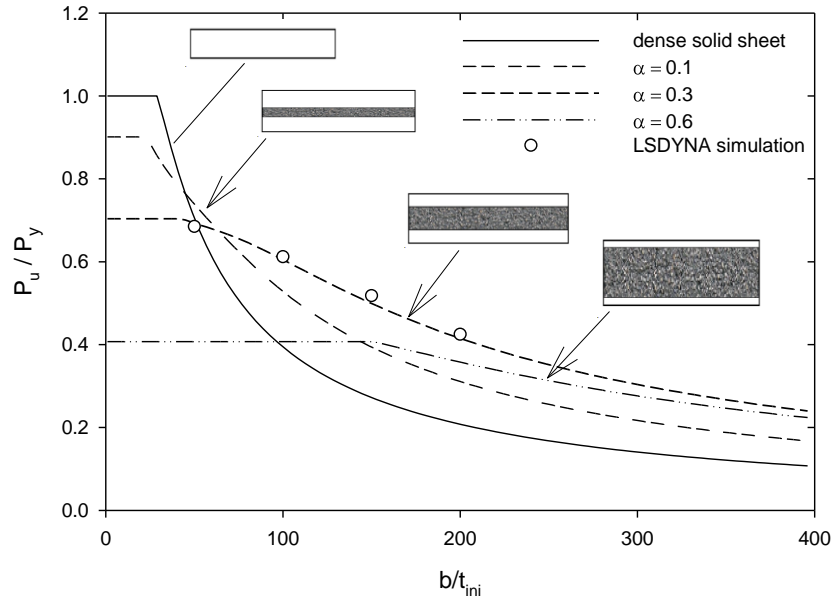


Figure 19: Buckling strength of solid steel and sandwich panels which have the same weight, 18% relative density hollow spheres foam cores, and variable depth of foaming. The plot shows buckling strength normalized against yield strength vs initial plate width-to-thickness.

6. Conclusions

It is shown that starting with just a few experimental tests, a database may be developed for any metal foam such that an organization may select the mechanical properties they desire from a wide range of possible values, and then manufacture a metal foam that will deliver those properties. The results from experimental tests are used to validate microstructural simulations, with which sensitivity analyses may then be run to predict mechanical properties of similar metal foams. Further such simulations could be performed to develop a full database of manufacturing parameters required to produce a metal foam of given mechanical properties, within the range of what is possible for a given production method.

By feeding the results from microstructural simulations into a constitutive model in a component-scale finite element analysis, the development of an optimal steel foam sandwich panel is demonstrated. This optimal sandwich panel possesses properties highly advantageous compared to solid steel, showing that steel foam has strong potential applications in the structural engineering realm.

Acknowledgments

The authors wish to acknowledge the financial support of the United States National Science Foundation (NSF) through grants CMMI-1000334, 1000167, 0970059. This research was also supported by the NSF through TeraGrid resources under grant number TG-MSS110026. The authors also wish to thank Drs. Hartmut Goehler and Guenter Stephani of the Fraunhofer Institute for Advanced Materials for preparing the hollow spheres foam, as well as Dr. Raouf Loutfy of MER Corporation for preparing the PCM foam.

References

- Andrews, E.W., Gioux, G., Onck, P., Gibson, L.J. (2001). "Size effects in ductile cellular solids. Part II: experimental results." *International Journal of Mechanical Science*, Elsevier, 43 701-713.
- Ashby, M.F., Evans, A.G., Fleck, N.A., Gibson, L.J., Hutchinson, J.W., Wadley, H.N.G. (2000). *Metal Foams: A Design Guide*. Butterworth Hamilton, Boston, MA.
- Deshpande, V., Fleck, N.A. (2000). "Isotropic constitutive models for metallic foams." *Journal of the Mechanics and Physics of Solids*, Elsevier, 48 1253-1283.
- Fallet, A., Lhuissier, P., Salvo, L., Brechet, Y. (2008). "Metallic Hollow Spheres Foam: Structure and Mechanics ." *Advanced Engineering Materials*, Wiley, 10 (9) 858-862.
- Friedl, O., Motz, C., Peterlik, H., Puchegger, S., Reger, N., Pippan, R. (2007). "Experimental investigation of mechanical properties of metallic hollow sphere structures." *Metallurgical and Materials Transactions, TMS / ASM International*, 39-1 135-146.
- Gao, Y.Z., Yu, T.X., Karagiozova, D. (2007). "Finite element simulations on the mechanical properties of MHS materials." *Acta Mechanica Sinica*, CSTAM, 23 65-75.
- Gao, Y.Z., Yu, T.X., Zhao, H. (2008). "Mechanical behavior of metallic hollow sphere materials: experimental study." *Journal of Aerospace Engineering*, ASCE, 21 (4) 206-216.
- Hanssen, A. Hopperstad, O., Langseth, M., Iltstad, H. (2002). "Validation of constitutive models applicable to aluminium foams." *International Journal of Mechanical Science*, Elsevier, 44 359-406.
- Kansal, A.R., Torquato, S., Stillinger, F.H. (2002). "Computer generation of dense polydisperse sphere packings." *The Journal of Chemical Physics*, AIP, 117 (18) 8212-8218.
- Kari, S., Bergerm, H., Rodriguez-Ramos, R., Gabbert, U. (2007). "Computational evaluation of effective material properties of composites reinforced by randomly distributed spherical particles ." *Composite Structures*, Elsevier, 77 223-231.
- Khan, A. (1995). *Continuum Theory of Plasticity*, Wiley Publishing, New York City.
- Miller, R.E. (2000). "A continuum plasticity model for the constitutive and indentation behaviour of foamed metals." *International Journal of Mechanical Science*, Elsevier, 42 729-754.
- Reyes, A. (2003). "Constitutive modeling of aluminum foam including fracture and statistical variation of density ." *European Journal of Mechanics A/Solids*, Elsevier, 22 815-835.
- Smith, B.H., Szymszewski, S., Hajjar, J.F., Schafer, B.W., Arwade, S.R. (2012). "Steel Foam for Structures: A Review of Applications, Manufacturing, and Material Properties." *Journal of Constructional Steel Research*, Elsevier, 71 1-10.
- Tuchinsky, L. (2005). "Novel Fabrication Technology for Metal Foams." *Journal of Advanced Materials*, SAMPE, 37 (3) 60-65.
- Woutense, A., Philipse, A.P. (2006). "Geometrical cluster ensemble analysis of random sphere packings." *The Journal of Chemical Physics*, AIP, 125 (19) 194709-194719.